Biogeosciences

Carbonate system in the water masses of the Southeast Atlantic sector of the Southern Ocean during February and March 2008

M. González-Dávila[1], **J. M. Santana-Casiano**[1], **R. A. Fine**[2], **J. Happell**[2], **B. Delille**[3], **and S. Speich**[4]

[1]Departamento de Química, Facultad de Ciencias del Mar, Universidad de Las Palmas de Gran Canaria, 35017, Spain
[2]Rosenstiel School, University of Miami, 4600 Rickenbacker Causeway, Miami, FL 33149-1098, USA
[3]Unité d'Oceanographie Chimique, Astrophysics, Geophysics and Oceanography department, University of Liège,
Allée du 6 Août, 17 (Bât B5), 4000 Liège, Belgium
[4]Laboratoire de Physique des Oceans (LPO), CNRS/IFREMER/UBO, Brest, France

Abstract. Carbonate system variables were measured in the South Atlantic sector of the Southern Ocean along a transect from South Africa to the southern limit of the Antarctic Circumpolar Current (ACC) from February to March 2008. Eddies detached from the retroflection of the Agulhas Current increased the gradients observed along the fronts. Minima in the fugacity of CO_2, $f CO_2$, and maxima in pH on either side of the frontal zone were observed, noting that within the frontal zone $f CO_2$ reached maximum values and pH was at a minimum.

Vertical distributions of water masses were described by their carbonate system properties and their relationship to CFC concentrations. Upper Circumpolar Deep Water (UCDW) and Lower Circumpolar Deep Water (LCDW) offered $pH_{T,25}$ values of 7.56 and 7.61, respectively. The UCDW also had higher concentrations of CFC-12 ($>0.2\,\mathrm{pmol\,kg^{-1}}$) as compared to deeper waters, revealing that UCDW was mixed with recently ventilated waters. Calcite and aragonite saturation states (Ω) were also affected by the presence of these two water masses with high carbonate concentrations. The aragonite saturation horizon was observed at 1000 m in the subtropical area and north of the Subantarctic Front. At the position of the Polar Front, and under the influence of UCDW and LCDW, the aragonite saturation horizon deepened from 800 m to 1500 m at 50.37° S, and reached 700 m south of 57.5° S. High latitudes proved to be the most sensitive areas to predicted anthropogenic carbon increase. Buffer coefficients related to changes in $[CO_2]$, $[H^+]$ and Ω with changes in dissolved inorganic carbon (C_T)

and total alkalinity (A_T) offered minima values in the Antarctic Intermediate Water and UCDW layers. These coefficients suggest that a small increase in C_T will sharply decrease the status of pH and carbonate saturation. Here we present data that suggest that south of 55° S, surface water will be under-saturated with respect to aragonite within the next few decades.

1 Introduction

The Southern Ocean plays an important role in modulating the global climatic system by transporting and storing heat, fresh water, nutrients, and anthropogenic carbon dioxide (CO_2) (e.g., Lovenduski and Gruber, 2005). This region is predicted to be greatly influenced by global change, given that polar marine ecosystems are particularly sensitive to carbonate change (Sarmiento et al., 1998; Orr et al., 2005). Since pre-industrial times, the uptake of CO_2 has modified the chemistry of the ocean, lowered the pH and the concentration of carbonate ions (CO_3^{2-}) with high latitudes among the most affected areas (Caldeira and Wickett, 2003; Orr et al., 2005). Surface ocean pH levels have already decreased by 0.1 units in the Southern Ocean (McNeil and Matear, 2007; Key et al., 2004) and are projected to decline by around 0.3 until the year 2100 (McNeil and Matear, 2008). Orr et al. (2005) predicted that the Southern Ocean will begin to experience aragonite under-saturation by the year 2050. On the other hand, there is a study by McNeil and Matear (2008) which is based on a large-scale Southern Ocean observational analysis that also considers the seasonal magnitude and variability of CO_3^{2-} and pH. This study suggests that the Southern Ocean aragonite under-saturation in

winter will already occur by the year 2030. As the dissolution of anthropogenic carbon increases, the total inorganic carbon concentration of the surface waters, and the capability to buffer these inputs decreases. This results in a much greater sensitivity to local variations in total inorganic carbon and total alkalinity. The lowest buffer values have been observed in the Southern Ocean (Egleston et al., 2010), as this area is particularly sensitive to increased CO_2.

The Southern Ocean is particularly efficient when ventilating deep and bottom waters (e.g. Toggweiler et al., 2006). Deep ventilation takes place south of the Polar Front (PF). There are clear links between the seasonal carbon dynamics and the Antarctic Bottom Water (AABW) formation regions (McNeil et al., 2007). The entrainment and upwell of Circumpolar Deep waters, rich in dissolved inorganic carbon and carbonate poor, into the surface layer lowers the carbonate concentration considerably (McNeil and Matear, 2008). A recent study showed that the upwelling of deep waters, rich in CO_2, is the most dominant driver of winter carbon cycling, as compared to temperature-driven differences in solubility or biological processes (McNeil et al., 2007). Physical processes such as deep-water formation in the Weddell Sea, the upwelling of deep water in the divergence zone and the formation of intermediate water in the Antarctic Polar Zone (APZ) affect the carbonate system parameters, with consequences for the CO_2 air-sea fluxes. In this region where several frontal systems are observed, sharp gradients in temperature and salinity (Lutjeharms and Valentine, 1984; Belkin and Gordon, 1996) and important changes in the CO_2 air-sea exchange have been described (Bakker et al., 1997; Hoppema et al., 1995; Chierici et al., 2004; McNeil et al., 2007).

In the framework of the BONUS-GoodHope project, the parameters of the carbonate system, pH, total alkalinity (A_T) and total dissolved inorganic carbon concentration (C_T) were measured in the southeast Atlantic sector of the Southern Ocean (Fig. 1). The main objective of this work was to characterise the carbonate system of the water masses present in the area, and determining their sensitivity to an increase of CO_2 in this sector of the Southern Ocean.

2 Hydrography of the area of study

The region studied (Fig. 1) is described in detail in Chever et al. (2010), based on Gladyshev et al. (2008). It is divided into three main regimes, namely, the sub-tropical domain north of $40°$ S–$42°$ S, the Antarctic Circumpolar Current (ACC) between $40°$ S–$42°$ S and $55°$ S–$57°$ S, and the boundary region between the ACC and Weddell Gyre/the northern edge of Weddell Gyre (Park et al., 2001; Gladyshev et al., 2008). In this region, several frontal systems were described in a review by Orsi and Whitworth (2005), using potential temperature (θ), salinity and oxygen as indicators. These frontal zones were defined both by sharp changes in temperature and
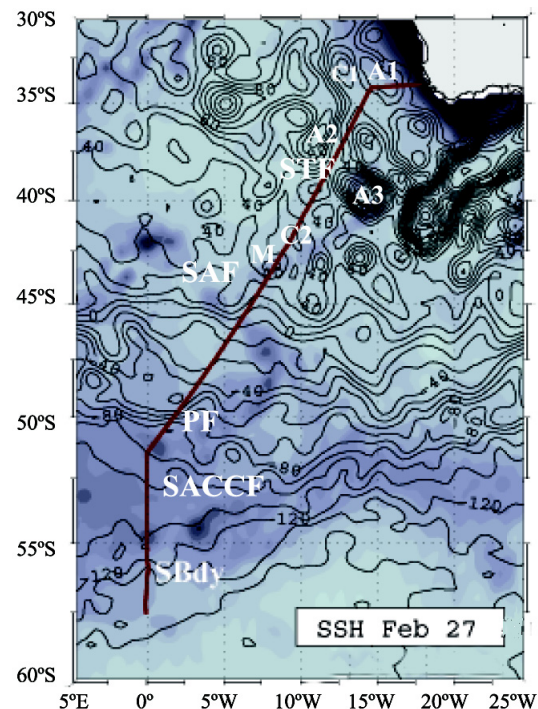

Fig. 1. Map showing the cruise track and sea surface height (SSH) for the southwest Atlantic sector of the Southern Ocean during the BONUS GoodHope 2008 cruise. The track is plotted over an altimetry image for 27 February and the fronts are identified: STF (Subtropical Front), SAF (Subantarctic Front), PF (Polar Front), SACCF (Southern ACC Front) and SBdy (Southern Boundary). Cyclonic (C_i) and anticyclonic (A_i and M) Agulhas rings are also marked.

salinity and by enhanced chlorophyll (Chl)-a concentrations and reduced values of partial pressure of CO_2 (expressed as fugacity of CO_2, fCO_2) (Smith and Nelson, 1986, 1990; Chierici et al., 2004; Laika et al., 2009). In the sub-tropical domain, the Sub-tropical Front (STF) divides the warmer tropical waters and the colder sub-Antarctic waters. The area is then divided by the North Sub-tropical Front (N-STF) and the South Sub-tropical Front (S-STF). The strong interaction between the Agulhas Current and slope and shelf waters in the Agulhas Bank (Boebel et al., 2003; Richardson 2007) produces the formation of cyclonic and anti-cyclonic Agulhas rings that strongly interact with fronts affecting their boundaries. These features are common in the Cape Basin and have been proved recently to define the position of the N-STF and S-STF (Dencausse et al., 2010).

In the ACC domain, four main fronts are identifiable. The Subantarctic Front (SAF) is located at around $44°$ S, with a sharp decrease in both salinity and temperature. The Polar Front, PF, is found at around $50°$ S, characterized by weak surface temperature and salinity gradients. A deep-reaching front observed to the south is indicative of the presence of the southern ACC front (SACCF), located at $52°$–$53°$ S. In

this region, the southern boundary of the ACC (SBdy) is located at around 56° S. During late summer, the position of this front cannot be detected by surface temperature gradients, but can be defined by an increase in salinity. South of the SBdy is the region of the Weddell Sea. The change from low salinity surface water in the ACC band to higher salinity waters is associated with the presence of the Weddell Gyre. The narrow band of more saline surface waters close to the frontal area comes from the upwelling of deep, salty water during the course of the water from the western part of the Weddell Gyre through to the Prime Meridian.

Along the transept, several water masses can be distinguished (see, e.g., Withworth and Nowlin, 1987; Arhan et al., 2011; Speich et al., 2011) as are briefly summarized here (Fig. 3). South of the SACCF at the SBdy, the Winter Water (WW) of the Antarctic Zone is observed as a sub-surface tongue centred at 150 m that extends northwards to the position of the Antarctic PF. In this region, two circumpolar deep waters (CDW) are distinguished: Upper Circumpolar Deep Water (UCDW) and Lower Circumpolar Deep Water (LCDW) (Whitworth and Nowlin, 1987). Circumpolar Deep Waters are a composite of deep waters flowing from the Indian, Atlantic and Pacific basins. When approaching the Antarctic Continent, these eventually mix with younger waters such as the Weddell Sea Deep Water (WSDW), WW and the Ice Shelf Water, forming the Modified CDW (M-CDW) or Antarctic Bottom Water (AABW). This mixing produces ventilated waters whose injection into mid-depth and bottom layers contributes to the ventilation of the deep Southern Ocean (Orsi et al., 2002; Lo Monaco et al., 2005; Bakker et al., 2008). Below 2000 m, influence of the WSDW can be discerned; the water mass originates from the Weddell Sea below about 1500 m. Below 4000 m, in the Agulhas basin, cores of CFC-rich waters identify the Antarctic Bottom Water (AABW), formed at several places around Antarctica (Orsi et al., 2002).

The near-surface water at the Antarctic Polar zone is the least saline near-surface water in the ACC band. It is observed continuously at all longitudes (Orsi and Whitworth, 2005). It subducts northwards at the SAF to feed the Antarctic Intermediate Water (AAIW), located in a 600–1000 m band further north. Moreover, the salinity maximum of the deep water northwards to the SAF is associated with the diluted North Atlantic Deep Water (NADW) (Arhan et al., 2003).

3 Data and methods

The BONUS-GoodHope cruise took place on board the French R/V *Marion Dufresne* in the southeast Atlantic sector of the Southern Ocean in the region 33°58′ S-57°33′ S, 17°13′ E–0° E (Fig. 1). It started on 13 February 2008, off Cape Town, and was completed on 17 March 2008. During the cruise, full depth CTD data were registered at 79 stations and samples were taken at 22 depths for the measurements of salinity, oxygen, pH, A_T and C_T. Oxygen concentrations were measured on board by Winkler titration. Chlorophyll-a (Chl-a) was also measured on board by fluorometric analysis of acetone (90 %) extracts (Speich and Dehairs, 2008). Samples were collected for the posterior laboratory analysis of two chlorofluorocarbons, CFC-11 and CFC-12.

The three variables of the carbonate system were measured on board the Marion Dufresne in order to achieve the highest level of data quality and resolution. The hydrocast stations (78 stations plus station zero) were sampled for pH on total scale at 25 °C (pH$_{T,25}$, with [H$^+$] in µmol kg^{-1}), total alkalinity (A_T, in µmol kg^{-1}) and total dissolved inorganic carbon concentration (C_T, in µmol kg^{-1}). There were a total of 1639 bottles in hydrocast CTD stations at non-repetitive depths, and in some cases samples were flagged. As a result, high quality data are available for pH from 1609 samples, from 1559 samples for A_T and from 1504 samples for C_T.

3.1 Sampling procedure

500 ml glass bottles were used for the analytical determination of both pH and A_T. 100 ml glass bottles were used to analyse C_T. The bottles were rinsed twice with seawater and were overfilled with seawater. Samples were shielded from the light and analysed between stations. At shallow stations and when samples could not be analysed for C_T in less than 6 h after sampling, they were poisoned with HgCl$_2$ (60 µl, saturated solution).

3.2 pH measurements

We measured pH on the total scale (pH$_T$) at a constant temperature of 25 °C (pH$_{T,25}$). An automated system based on the spectrophotometric technique of Clayton and Byrne (1993) with m-cresol purple as an indicator (the dye effect was removed for each pH reading) and with an uncertainty of 0.002 units was used (González-Dávila et al., 2003).

3.3 Total dissolved inorganic carbon measurements

A VINDTA 3C system (Mintrop et al., 2000) (www. MARIANDA.com), with coulometer determination was used for the titration of total dissolved inorganic carbon concentration after phosphoric acid addition. The titration of certified reference material for oceanic CO$_2$, CRMs (#85), supplied by Andrew Dickson at Scripps Institution of Oceanography, was used to test the performance of the equipment. A CRM was analysed every time a new titration cell for C_T determination was prepared (once a day); in total 31 CRMs were analysed. We measured 1996.0 ± 1.6 µmol kg^{-1} for C_T, while the certified value is 2000.4 ± 0.4 µmol kg^{-1}. A study done on board indicates that this difference relates to the temperature at which C_T is determined which was 25 °C in our case. Raw data were corrected for this offset by

multiplying by the factor 1.0022. Each CRM sample was also analysed for total alkalinity.

3.4 Total alkalinity measurements

Samples for A_T were potentiometrically titrated with standardized 0.25 M HCl (0.45 M in NaCl) to the carbonic acid end point using a titration system described in detail in Mintrop et al. (2000). The titration of CRMs (#85) was used to test the performance of the titration system. Measurements of CRMs were within $\pm 1.1\,\mu mol\,kg^{-1}$ of the certified value. The agreement between on board experimental data of A_T (2184.0 ± 1.1) and the certified value (2184.0 ± 0.8) indicates accurate HCl concentration and pipette volume for the titration system. No correction was carried out on the experimental data.

3.5 CFC sampling and measurement

1191 samples (a mean of 18 samples per hydrocast) were collected from Niskin bottles. The samples (about 125 ml) were taken via Viton tubes connected to glass bottles with connectors. The bottles and caps were thoroughly rinsed with the water to be sampled. The bottles were filled and capped underwater in a 1 l beaker. At the University of Miami laboratory, water samples were analysed for CFC-11 and CFC-12 using an extraction system and gas chromatograph following established procedures (Bullister and Weiss, 1988). Analytical uncertainties for CFC-11 (CCl_3F) and CFC-12 (CCl_2F_2) are each $\pm 8\,\%$.

3.6 Calculations

3.6.1 Calcite and aragonite saturation state

The saturation state of seawater with respect to calcite and aragonite (Ω) was calculated as the product of the calcium (Ca^{2+}) and carbonate ion (CO_3^{2-}) concentrations at in situ temperature, and the salinity and pressure, divided by the stoichiometric solubility product (K_{sp}^*) for those compounds

$$\Omega_{cal} = [Ca^{2+}][CO_3^{2-}]/K_{sp,cal}^* \tag{1}$$

$$\Omega_{ara} = [Ca^{2+}][CO_3^{2-}]/K_{sp,ara}^* \tag{2}$$

where the calcium concentration is estimated from salinity (Lewis and Wallace, 1998), and the carbonate ion concentration is calculated from A_T and C_T, and computed by using CO2sys.xls v12 (Lewis and Wallace, 1998), using the carbonic acid dissociation constants of Mehrbach et al. (1973) as in Dickson and Millero (1987), the sulphate dissociation constant by Dickson (1990a) and the K_{sp}^* from Mucci (1983). Other values are described in detail in Lewis and Wallace (1998). The nutrient data were considered in all the computations (Speich and Dehairs, 2008; Branellec et al., 2010).

3.6.2 Normalisation procedure

The pH_T at in situ conditions (pH_{Tis}) was computed by applying the CO2sys.xls v12 programme and the set of constants mentioned above, to the experimental $pH_{T,25}$ and A_T pairs of data. The nutrient data were also considered.

The regional normalisation to a constant salinity (S^{ref}) proposed by Friis et al. (2003) was applied to the alkalinity and inorganic carbon concentration (X_T), instead of the traditional normalisation $N X_T = X_T/S^{mea} \cdot S^{ref}$, where S^{mea} is the salinity measured. This alternative procedure removes the effects of evaporation and precipitation as well as the salinity-proportional parts of mixing/upwelling and non-zero end-member, and improves the interpretation of their variations in the water column. In this normalisation, the salinity adjustment is based on a constant and region-specific term for $S = 0$, which expresses river run-off, upwelling from below the lysocline, calcification, and lateral sea surface-water exchange.

$$N X_T = (X_T^{mea} - X_T^{S=0})/S^{mea} \cdot S^{ref} + X_T^{S=0} \tag{3}$$

Our surface data for A_T and C_T were fitted to the equation $X_T = m_T T + m_S S + b^0$,

$$A_T = -3.18(\pm 0.17)T + 59.95(\pm 1.65)S + 266.6(\pm 55.4) \tag{4}$$

$$C_T = -10.49(\pm 0.14)T + 41.97(\pm 1.40)S + 757.4(\pm 46.9) \tag{5}$$

with standard error of estimate of ± 5.14 and ± 4.88 for A_T and C_T, respectively. According to Eqs. (4) and (5), $A_T^{S=0} = 266.6 \pm 55.4$ and $C_T^{S=0} = 663.1 \pm 122.6$. S^{ref} was fixed to the traditional salinity of 35.

3.6.3 Buffer coefficients

The explicit expressions for seven buffer factors that quantify the ability of ocean chemistry to resist changes in dissolved inorganic carbon and alkalinity as a function of proton, carbonate and borate ion concentrations were computed following Egleston et al. (2010), using their Table 1. Calculations of the several parameters used in these expressions were obtained after applying CO2sys program to pairs of data of C_T and A_T, assuming the set of constants indicated above. Six of those factors quantify the sensitivity of $[CO_2]$ (γ_i), $[H^+]$ (β_i) and Ω (ω_i) to changes in dissolved inorganic carbon concentration (C_T) and alkalinity (A_T), while β_H refers to the traditional buffer capacity of the system, quantifying the resistance to changes of the pH of a chemical system to additions of a strong acid or base and it equals to $-2.3\,\beta_{A_T}$.

We have defined $Q = [HCO_3^-] + 4[CO_3^{2-}] + [H^+][B(OH)_4^-]/(K_b + [H^+]) + [H^+] - [OH^-]$, where K_b is the acidity constant for boric acid (Dickson, 1990b); P $= 2[CO_2] + [HCO_3^-]$; $A_c = [HCO_3^-] + 2[CO_3^{2-}]$. In order to avoid confusion, noted that the letter Q was used instead of S in the Egleston et al. (2010) paper.

$$\gamma C_T = \left(\frac{\partial \ln[CO_2]}{\partial C_T}\right)^{-1} = C_T - \frac{A_c^2}{Q}$$

$$\gamma A_T = \left(\frac{\partial \ln[CO_2]}{\partial A_T}\right)^{-1} = \frac{A_c^2 - C_T \cdot Q}{A_c}$$

$$\beta C_T = \left(\frac{\partial \ln[H^+]}{\partial C_T}\right)^{-1} = \frac{C_T \cdot Q - A_c^2}{A_c}$$

$$\beta A_T = \left(\frac{\partial \ln[H^+]}{\partial A_T}\right)^{-1} = \frac{A_c^2}{C_T} - Q$$

$$\omega C_T = \left(\frac{\partial \ln\Omega}{\partial C_T}\right)^{-1} = C_T - \frac{A_c \cdot P}{[HCO_3^-]}$$

$$\omega A_T = \left(\frac{\partial \ln\Omega}{\partial A_T}\right)^{-1} = A_c - \frac{C_T \cdot [HCO_3^-]}{P} \qquad (6)$$

4 Results and discussion

4.1 Surface distribution

During the BONUS-GoodHope cruise, the expected trend of decreasing surface temperature towards the south was observed indeed (Fig. 2). This temperature gradient accompanied a decrease in $pH_{T,25}$ and an increase in the surface dissolved inorganic carbon concentrations C_T (Fig. 2). By using Sea Surface Temperature (SST) and Sea Surface Salinity (SSS) data from this research and the definitions of the characteristics of the major fronts south of Africa, the five major oceanic frontal structures have been identified and are marked in Fig. 2. The south Subtropical Front (S-STF) was located at 42°2′ S. The north Sub-tropical Front (N-STF) was located west of the cruise line at around 38° S (Chever et al., 2010). SST drops from 20.95 °C at 37.7° S to 15.31 °C at 38.83° S, while SSS decreases from 35.52 to 34.6. At those latitudes, the cruise crossed a warm, saltwater layer of two Agulhas rings at their boundaries. These were located at 36° S–38° S (A2) and 35° S (A1), respectively (see Fig. 1). The influence of a cyclonic ring close to 36° S (C1) increased the gradient observed in this region. The cyclonic structure C1 was injected into the region from the African slope (from the Agulhas Bank) as can be seen both from tracking using satellite altimetry (Fig. 1) and its hydrologic characteristics (e.g., salinity, oxygen, Fig. 3).

From 41.60° S to 42.03° S, at the S-STF, the SST values dropped from 15.64 to 12.06 °C and the SSS fell from 34.75 to 34.22. From 39.2° S to 40.2° S, SSTs as high as 17 °C and SSS of 35 were found to be related to the influence of another Agulhas ring (A3), centred at 40° S, 14° E (Fig. 1). The changes in both temperature and salinity also affected the carbonate system variables which can also be used to distinguish the presence of the fronts. At around 38° S, the presence of the Agulhas rings in the 36° S–38° S (A1, C1 and A2) increased the $pH_{T,25}$ from 7.97 at
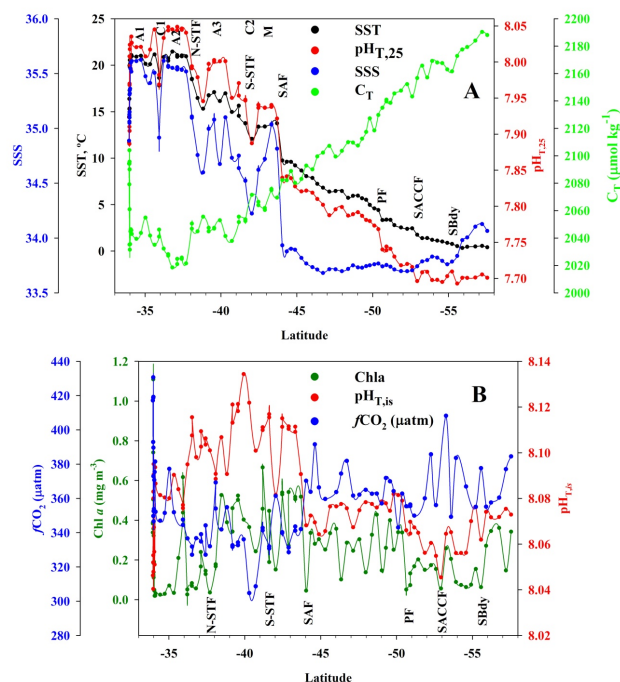

Fig. 2. (A) The sea surface temperature (SST), salinity (SSS), total dissolved inorganic carbon (C_T, µmol kg^{-1}) and pH in total scale at 25 °C ($pH_{T,25}$) along the cruise track for samples analysed over the upper 10 m. The figure shows the position of the major frontal zones during the BONUS GoodHope cruise. **(B)** Surface ocean Chlorophyll a, partial pressure of CO_2 in seawater expressed as fugacity, $fCO_{2,sw}$ (µatm) and pH in total scale at in situ conditions, pH_{Tis}.

36° S to 8.040 all along 36.5° S to 37.8° S. Between A2 and A3, the $pH_{T,25}$ shifted from 8.040 to 7.946, increasing to 7.97 at the position of the anticyclonic ring A3. At the S-STF, the $pH_{T,25}$ decreased from 7.948 to 7.887, indicating a total change inside the STF area of 0.15 pH units. Again, from 39.2° S to 40.2° S, the $pH_{T,25}$ increased from 7.95 to 8.00, in line with the observed temperature increase. Total alkalinity was strongly correlated with salinity. A_T (data not shown) decreased from 2334 to 2296 µmol kg^{-1} at 38° S, between rings A2 and A3. The A_T from 41.60° S to 42.03° S at the S-STF, dropped from 2294 µmol kg^{-1} to 2273 µmol kg^{-1}. There was also a noticeable increase in C_T at both locations with changes of 33 µmol kg^{-1} at the 38° N (from 2018.2 to 2051.6 µmol kg^{-1}) and around 20 µmol kg^{-1} at the southern front, increasing from 2051.1 µmol kg^{-1} to 2072.8 µmol kg^{-1}. After normalisation to a constant salinity (data not shown), the NC_T increased by 70 µmol kg^{-1} at 38° N and 31 µmol kg^{-1} at the S-STF. These variations indicate that the upwelling of deep CO_2-rich waters takes place in this frontal area that, at least at the time of the cruise, overcompensates any reduction of CO_2 due to biological activity. An examination of Fig. 3 suggests a deep-reaching nature of the STF related to the presence of the Agulhas rings detached from the retroflection of the Agulhas Current.
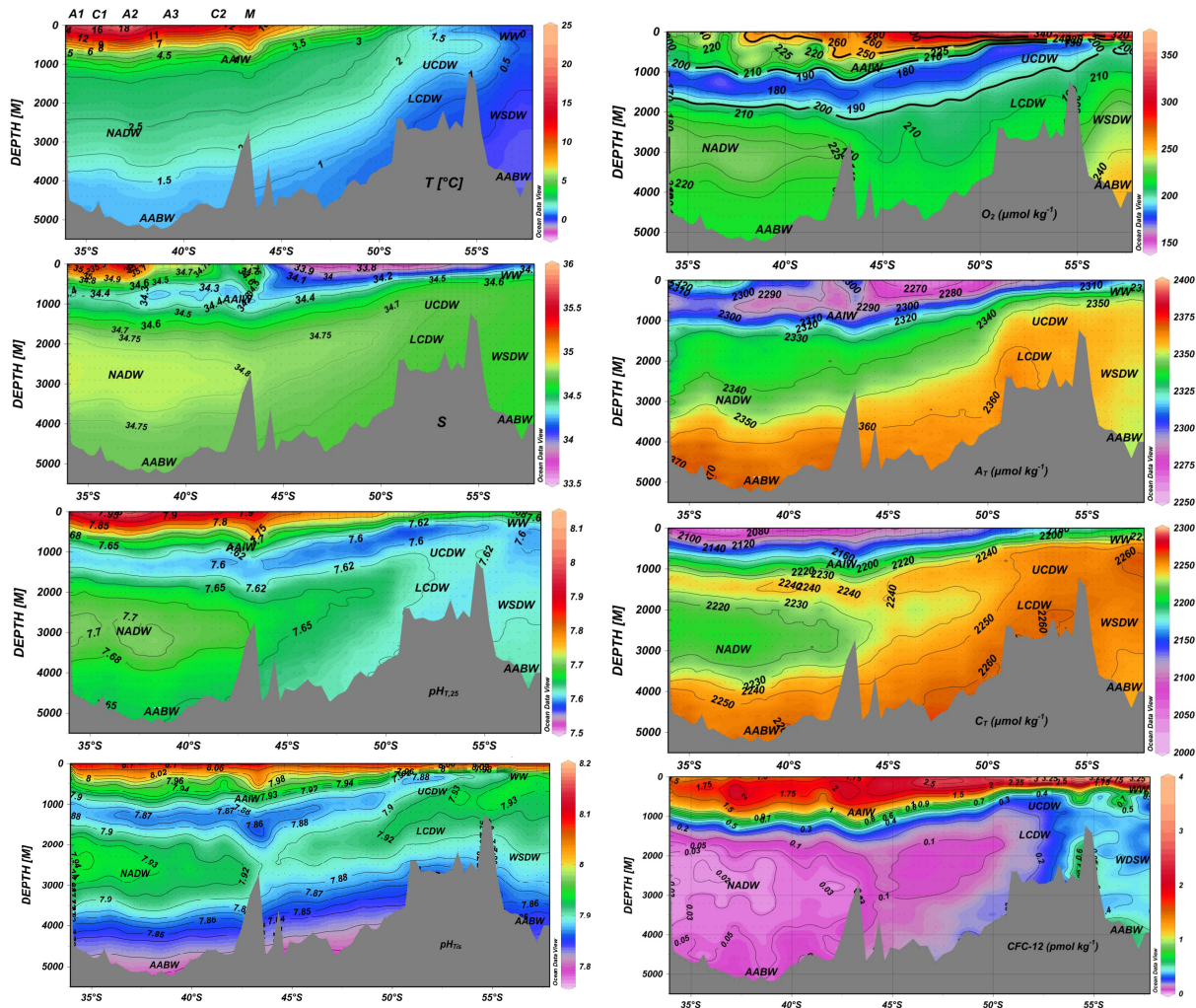
Fig. 3. The vertical distribution of temperature (T, °C), salinity (S), pH in total scale at 25 °C (pH$_{T,25}$), pH in total scale at in situ conditions (pH$_{Tis}$), dissolved oxygen (O_2, µmol kg^{-1}), total alkalinity (A_T, µmol kg^{-1}), total dissolved inorganic carbon (C_T, µmol kg^{-1}) and chlorofluorocarbon-12 (CFC-12, pmol kg^{-1}) along the southeast Atlantic sector of the Southern Ocean during February to March 2008. The dots indicate the locations of discrete samples.

In the ACC domain, four main fronts were identified. The Sub-Antarctic Front (SAF) was located at 44°2′ S. The SSS dropped from 35.037 at 43°19′ S to 33.93 at 44°2′ S and the SST fell from 13.74 to 9.74 °C, located barely south of an old intense Agulhas Ring (M in Fig. 1). At these positions, the pH$_{T,25}$ sharply decreased by 0.1 pH units from 7.938 to 7.839, the A_T dropped from 2314 to 2265 µmol kg^{-1} while the C_T increased from 2070 to 2082 µmol kg^{-1}. The Polar Front, PF, was located at 50°22′ S. A significant pH$_{T,25}$ gradient was observed at the front changing from 7.768 to 7.740. The total alkalinity increased by 7 µmol kg^{-1} from 2280 µmol kg^{-1} while the C_T increased by 10 µmol kg^{-1} from 2130 µmol kg^{-1} at 50°22′ S to 2140 µmol kg^{-1} at 50°38′ S.

The southern ACC front (SACCF), was charted at 52°39′ S. At this front, the SST slightly decreased from

2.44 °C at 52°36′ S to 1.75 °C at 52°55′ S while the SSS increased from 33.705 to 33.742. The position of the SACCF is seen more precisely on the pH gradient, with the pH$_{T,25}$ decreasing from 7.716 to 7.696 as we moved southwards. At these positions, the C_T increased by 13 µmol kg^{-1} from 2143 µmol kg^{-1} at 52°36′ S to 2157 µmol kg^{-1} at 52°55′ S. In the region studied, the southern boundary of the ACC (SBdy) was located at 55°54′ S. It was detected by the increase in salinity from 33.836 at 55°34′ S to 33.980 at 55°54′ S. At that position, the A_T increased from 2293 µmol kg^{-1} to 2308 µmol kg^{-1}. After normalisation, the NA_T is still 4 µmol kg^{-1} higher related to the upwelling of deep water rich in alkalinity.

From the pH$_T$ at in situ conditions (pH$_{Tis}$) computed fugacity of CO_2, $fCO_2(A_T, C_T)$, and the Chl-a (Fig. 2b), we can see that the highest pH and lowest fCO_2 values were

observed in the same areas where there were Chl-*a* maxima. Along the section, there appeared to be two regions with different mean conditions for pH_{Tis} and $f CO_2$. North of the SAF, a mean pH_{Tis} value of 8.102 ± 0.014 with $f CO_2$ of 335 ± 5 µatm was observed, while to the south, the pH_{Tis} was 8.069 ± 0.008 and the $f CO_2$ increased to 365 ± 10 µatm. The undersaturation observed in the sub-tropical zone with $f CO_2$ values below atmospheric (378 µatm, see Speich and Dehairs, 2008 for details) is in concordance with the strong sink for atmospheric CO_2 previously described for the area (Siegenthaler and Sarmiento 1993, Metzl et al., 1995; Brévière et al., 2006; Borges et al., 2008). The observed Chl-*a* concentration varied between 0.06 and 0.67 mg m^{-3}. In general, elevated Chl-*a* levels (reaching 0.4 and 0.6 mg m^{-3}) were associated with the shear area of the frontal zone, with very low values (below 0.2 mg m^{-3}) around the position of the rings. They were accompanied by minima of $f CO_2$ (e.g., 332 µatm at 38° N) and maxima of pH_{Tis} (e.g., 8.107 at 38.1° S) on either side of the frontal zone, while at the position of the frontal zone, the $f CO_2$ was at a maximum (369 µatm at the 38° S area) and the pH_{Tis} was at a minimum (8.088, at 38° S) (Fig. 2b). At the positions of the fronts, surface nitrate concentrations (data not shown) moved from below detection limit to north of 38.1° S to 3.22 µmol kg^{-1} south and from 4.94 µmol kg^{-1} at 41.60° S to 10.19 µmol kg^{-1} at 42.03° S, under the influence of eddy C2. This implies that mixing takes place at the frontal zones, in particular where cyclonic rings are located, bringing up CO_2-rich (plus low pH and high nutrient) water that spreads out over the fronts where recent biological production favoured by the nutrient input increased the pH_{Tis} and decreased the $f CO_2$ levels. Eddies and rings provided the conditions to promote primary production, as has been indicated in the case of the Haida eddies (Crawford et al., 2005) and in other areas including oligotrophic areas (McGillicuddy et al., 2003; Pelegrí et al., 2005; González-Dávila et al., 2006). A special event was observed south of 40° S at the southern limit of the two detached Agulhas rings. Strong $f CO_2$ under-saturation was detected together with high pH values and low Chl-*a* values. These may be the result of a chemical memory effect indicating previous primary production, which was over at the time of sampling (and where Chl-*a* was thus, low again).

South of 44° S, the Southern Ocean surface waters were rich in nutrients (nitrate values >16 µmol kg^{-1} that increased to >25 µmol kg^{-1} south of the PF) but low in Chl-*a* (Fig. 2b), typically referred to as high-nutrient-low-chlorophyll (HNLC) waters. The primary production is not able to take up macronutrients in these areas due to iron limitation, unstable surface-water stratification, and light limitation, defined as being responsible for the maintenance of the HNLC condition in the ice-free Southern Ocean (e.g., Venables and Moore, 2010).

Surface water alkalinity for the area between 30° S and 70° S and with SST < 20 °C and 33 < SSS < 36 in the South-

ern Ocean can be estimated by the following relationship Eq. (7) (Lee et al., 2006):

$$A_T = 2305 + 52.48(SSS - 35) + 2.85(SSS - 35)^2$$
$$- 0.49(SST - 20) + 0.086(SST - 20)^2 \qquad (7)$$

The mean difference ΔA_T (measured - calculated) between values calculated using thes relationship and our measured values was -3.4 ± 5.1 µmol kg^{-1}. The largest differences (−8.2) were observed at 40°17′ S, between the two northern Agulhas Rings (St 17 and 34), where cyclonic rings C1 and C2 were located, at the Polar Front (St 80) and south of the SBdy area. If these areas are removed, ΔA_T is -2.5 ± 4.3 µmol kg^{-1}. This result confirms both the validity of the relationship provided by Lee et al. (2006) for the full region except were mesoscale structures were observed, and that the surface alkalinity stays constant under CO_2 uptake by the ocean, at least in the short-to-mid-term future (e.g., Orr et al., 2005).

4.2 Carbonate system characteristics

The oceanic region separating the African and Antarctic continents has been less studied than its two counterparts south of South America (the Drake Passage) and south of Australia. Recent observations from this region have significantly improved our knowledge of the properties and circulation of water masses exiting and entering the Atlantic Ocean south of Africa and processes influencing the Agulhas leakage (Hoppema et al., 2000; Richardson et al., 2003; Van Aken et al., 2003; Gladyshev et al., 2008). However, the carbonate properties in this region have not been fully described (Lo Monaco et al., 2005; Bakker et al., 2008). Due to water mass formation and transformation taking place in the Southern Ocean near the continent and water transport (Orsi and Whitworth, 2005), we will describe the carbonate system properties and their relationship to the CFC concentrations from south to north.

South of the SACCF, the Winter Water (WW) of the Antarctic Zone is characterised by a sub-surface tongue centred at 150 m with CFC-12 concentrations exceeding 2.5 pmol kg^{-1} (Fig. 3). The vertical transition between WW and the Circumpolar Deep Water south of the Southern ACC Front is marked by a pronounced halocline at ∼200 m depth. The UCDW was characterised by a $pH_{T,25}$ as low as 7.56, (low $pH_{Tis} = 7.87$ and low oxygen, 175 µmol kg^{-1}) and the LCDW by high salinity and $pH_{T,25} = 7.61$ ($pH_{Tis} = 7.93$). Both the Circumpolar Deep Water masses are characterized by a maximum in C_T concentrations (2245–2260 µmol kg^{-1}, NC_T of 2270–2280 µmol kg^{-1}, from Eq. 3) attributed to the influence of old waters from the Indian and Pacific Oceans (Hoppema et al., 2000; Lo Mónaco et al., 2005). The UCDW is located in the 300–600 m range south of the PF with C_T of 2255 µmol kg^{-1} (NC_T of 2280 µmol kg^{-1}). This range of values compared well with those provided by Bakker et al. (2008) along 0° and from 55° S to 58° S. They found

C_T data in the 2250–2260 µmol kg^{-1} range at the 300–400 m range during December 2002. These values increased to over 2260 µmol kg^{-1} further south. The UCDW extends deeper north of the PF reaching 900–1500 m at 49° S with values of C_T in the range 2240–2245 µmol kg^{-1} (NC_T in the range of 2260 to 2265 µmol kg^{-1}) and low pH$_{Tis}$ (7.87). The UCDW has higher concentrations of CFC-12 (>0.2 pmol kg^{-1}) as compared to deeper waters also revealing the mixing with recently ventilated waters. The influence of the Weddell Sea Deep Water (WSDW) was detected below 2000 m and south of SBdy, with temperatures colder than 0 °C and salinities under 34.66. We found a pH$_{T,25}$ of 7.62 (pH$_{Tis}$ in the range 7.88–7.90), oxygen of 235 µmol kg^{-1} and C_T around 2250 µmol kg^{-1} in the WSDW. Close to the seafloor, the core of CFC-rich waters can be used to identify the presence of AABW (Mantisi et al., 1991; Orsi et al., 2002). The formation process of AABW also involves WW, Ice Shelf Water and deep waters of local origin including the Weddell Sea Deep Water (Wong et al., 1998), characterised by relatively high levels of CFC-12 >0.5 pmol kg^{-1}, and slightly higher oxygen (over 245 µmol kg^{-1}) and pH$_{T,25}$ values (7.63) than in WSDW, but lower pH$_{Tis}$ (below 7.85). A similar CFC distribution was also observed by Lo Mónaco et al. (2005) along 30° E in 1996.

The Antarctic Intermediate Water (AAIW), located at the 600–1000 m band is identified by the northward deepening of the salinity minimum at the near-surface waters of the Polar Frontal Zone, together with the deepening of C_T and CFC-12 isolines. AAIW in this region is characterized by low pH$_{T,25}$, ranging between 7.65 and 7.68 (pH$_{Tis} = 7.93$) but slightly higher than those at UCDW. The AAIW core followed the 27.1 to 27.4 potential density line moving to 600–800 m depth in the Cape Basin area, where it met the Indian AAIW injected with the Agulhas Rings. In the Cape Basin, salinity values were 0.2 units higher and the temperature was 2 °C warmer than at 45° S. The AAIW also had higher dissolved inorganic carbon content, ranging from 2170 µmol kg^{-1} at 45° S to values over 2185 µmol kg^{-1} in the Cape Basin, which also had lower CFCs than at 45° S, in accordance with Fine et al. (1988).

Along the northern part of the section, the deep salinity maximum is not associated with LCDW, but with diluted North Atlantic Deep Water. It has low CFC concentrations (<0.05 pmol kg^{-1}), as a sign of its age and its long passage across the Atlantic Ocean from its formation area. This water is one of the two NADW varieties found in the region. The present variety corresponds to the eastern NADW pathway that has crossed the South Atlantic at 20° S–25° S (Arhan et al., 2003) and then flows southeastward along the African slope as a slope current. It is usually found in the Cape Basin and north of the SAF. It is characterised by salinity maxima over 34.83. It is present as a uniform layer of pH$_{T,25} > 7.69$ (pH$_{Tis} = 7.93$), A_T in the range 2340 to 2350 µmol kg^{-1} (NA_T around 2355 µmol kg^{-1}) and C_T between 2210 and 2220 µmol kg^{-1} (NC_T between 2215 and 2225 µmol kg^{-1}).

The other variety of NADW is found south of the SAF in the APZ. It is characterised by salinity maxima between 34.74 and 34.79, and is associated with NADW injected in the ACC in the southwestern Argentine Basin (Whitworth and Nowlin, 1987). It should be regarded as a blend of LCDW and NADW injected into the ACC in the Argentine Basin. Concentrations of CFC-12 are in the range of 0.08 and 0.1 pmol kg^{-1}. The north to south uplifting of isolines showed the transition of water properties between mixed and pure LCDW water. South of 44° S, this NADW variety presented pH$_{T,25}$ between 7.66 and 7.67 (pH$_{Tis}$ of 7.90–7.91), A_T ranging between 2345 and 2360 µmol kg^{-1} (NA_T of 2365 and 2370 µmol kg^{-1}) and C_T in the range of 2230–2240 µmol kg^{-1}, corresponding to a NC_T of 2245 and 2255 µmol kg^{-1}.

AABW can also be distinguished in the deepest part of the section in the form of a layer of slightly higher CFC-12 values (>0.07 pmol kg^{-1}), low pH$_{T,25}$ and pH$_{Tis}$ (7.65 and 7.81) and high A_T and NA_T (2365–2370 and 2385–2388 µmol kg^{-1}), spreading north reaching 36° S. These values are lower for CFC-12 and slightly higher for C_T and lower for pH$_T$ than those shown above, south of the SBdy, indicating that this AABW is older and became diluted by the overlaying NADW from the south to the north, as indicated in Gladyshev et al. (2008).

Calcite and aragonite saturation states, Ω_{cal} and Ω_{ara}, (Fig. 4) decrease from north to south in the first 600 m. The isoline of $\Omega_{cal} = 2$ was located at 500–600 m in the subtropical area, dropping to under 700 m at the position of the old Agulhas ring M (the one located immediately north of the SAF), and reaching 100 m in the ACC zone, following what it has been shown by Hauck et al. (2010) on the same transect. The same vertical positions were followed for the isoline of $\Omega_{ara} = 1.2$. The influence of the UCDW and LCDW with higher carbonate ion concentration and older waters from the Indian and Pacific oceans maintained the Ω_{cal} over 1.5 at 1200–1500 m south of the APF, and the isoline of $\Omega_{cal} = 1.5$ at 1000 m north of the PF. Values below the calcite saturation horizon are located below 3800 m in the subtropical area, 3300–3400 m in the sub-Antarctic zone, and at around 3100–3200 m south of the SBdy. The aragonite saturation horizon is at 1000 m in the subtropical area and north of the SAF, as a result of the influence of eddy M, that presented decreased C_T values (2101 µmol kg^{-1} at 500 m) inside the eddy and higher values (2184 µmol kg^{-1} at 500 m) outside the eddy field. The presence of the PF together with the influence of the UCDW and the LCDW made the aragonite saturation horizon deepen from 800 m at 49.57° S to 1500 m at 50.37° S. South of this latitude, the position of the saturation horizon shoaled at 700 m at 57.5° S. This distribution should be strongly seasonally affected (McNeil and Matear, 2008) due to the ventilation of deeper waters in the Southern Ocean south of the PF as a result of upwelling, due to winter cooling and strong persistent winds. These deep waters are C_T rich and carbonate ion poor, lowering the carbonate
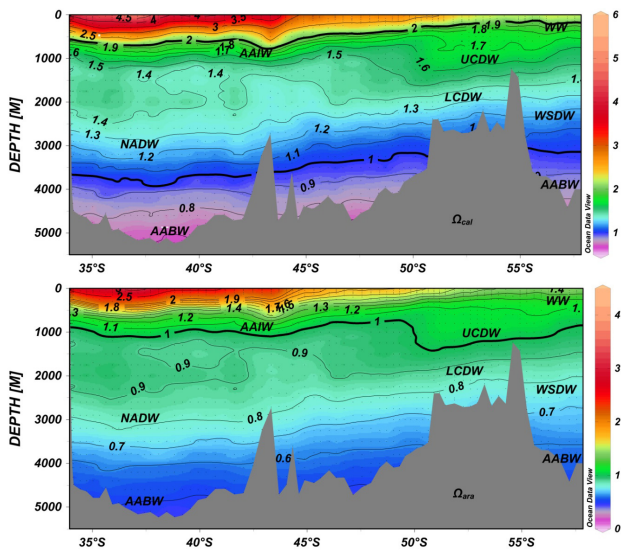
Fig. 4. The vertical distribution of the calcite saturation, Ω_{cal}, and aragonite saturation, Ω_{ara}, from February to March 2008 in the southeast Atlantic sector of the Southern Ocean. The calcite and aragonite saturation horizon is marked.

ion concentration considerably. During summertime (McNeil and Matear, 2008), the shallow mixed layers evolve where the biological production depletes the C_{T} and enriches carbonate ion concentrations. Subduction of these waters explains the vertical distribution of calcite and aragonite saturation states in the Polar sector observed during this cruise.

4.3 Sensitivity of carbonate system to increasing CO_2

The decrease in the carbonate ion concentration and the pH as a direct result of the increased CO_2 in the atmosphere and in the surface ocean affects and will continue to affect the ocean chemistry. In order to account for the sensitivity to future changes, we used the experimental data to compute the fractional changes in $[CO_2]$ (γ_i), $[H^+]$ (β_i) and Ω (ω_i) induced by changes in C_{T} and A_{T}. Following Frankingnoulle (1994) and updated by Egleston et al. (2010) (Eq. 6) seven buffer factors have been used to quantify the ability of the ocean to slow down changes in carbonate chemistry.

$$\gamma_{C_{\text{T}}} = (\partial \ln[CO_2]/\partial C_{\text{T}})^{-1}$$
$$\gamma_{\text{Alk}} = (\partial \ln[CO_2]/\partial \text{Alk})^{-1}$$
$$\beta_{C_{\text{T}}} = (\partial \ln[H^+]/\partial C_{\text{T}})^{-1}$$
$$\beta_{\text{Alk}} = (\partial \ln[H^+]/\partial \text{Alk})^{-1} = -\beta_{\text{H}}/2.3$$
$$\omega_{C_{\text{T}}} = (\partial \ln \Omega/\partial C_{\text{T}})^{-1}$$
$$\omega_{\text{Alk}} = (\partial \ln \Omega/\partial \text{Alk})^{-1} \qquad (8)$$

The buffer factors have dimensions of mol kg^{-1} of seawater (mmol kg^{-1} throughout the text). Low values imply low buffering capacity and larger changes in $[CO_2]$, $[H^+]$ and Ω for a given change in C_{T} or A_{T}. Rising atmospheric

CO_2 concentrations increase the C_{T} of the ocean, without changing its A_{T}. However, biological feedback including biogenic calcification or enhanced calcite dissolution and increased mineral weathering may increase the alkalinity, and thus the capacity to store CO_2 (Egleston et al., 2010). Figure 5 depicts the vertical distribution of the seven buffer coefficients over the Bonus GoodHope section. Figure 5 also shows the ratio of carbonate alkalinity to inorganic carbon A_c/C_{T}, which quantifies the number of protons released by CO_2 at the pH of the sample. Minimum absolute values for the buffer coefficients are found in waters with similar C_{T} and A_{T} values and pH of about 7.5. The presence of borate results in a minimum value not exactly located half-way between the two acidic constants for the carbonate system. In this region of pH (Santana-Casiano and González-Dávila, 2011), the CO_3^{2-}, CO_2 and $B(OH)_4^-$ are present at very low concentrations, and small additions of acid or base reacting with HCO_3^- strongly affect the concentration of CO_3^{2-}, CO_2, and pH. It should be noted that CO_2 additions leave the $[HCO_3^-]$ roughly constant while $[H^+]$ increases and $[CO_3^{2-}]$ decreases. Moreover, as $[Ca^{2+}]$ and the solubility products of calcium carbonate are invariant with changes in C_{T} and A_{T} (at constant salinity and temperature), $\omega_{C_{\text{T}}}$ and $\omega_{A_{\text{T}}}$ (see data and method section) describe how the $[CO_3^{2-}]$ changes with C_{T} and A_{T}, respectively. The values of $\gamma_{C_{\text{T}}}$ and $\beta_{C_{\text{T}}}$ are positive while $\omega_{C_{\text{T}}}$ is negative because the addition of CO_2 to the seawater increases $[CO_2]$ and $[H^+]$ but decreases $[CO_3^{2-}]$. Reversely, $\gamma_{A_{\text{T}}}$ and $\beta_{A_{\text{T}}}$ are negative while $\omega_{A_{\text{T}}}$ is positive because the addition of a strong acid (base) to seawater increases (decreases) $[CO_2]$ and $[H^+]$ but decreases (increases) $[CO_3^{2-}]$. As indicated in Egleston et al. (2010), the Revelle factor, R, can be computed as $R = C_{\text{T}}/\gamma_{C_{\text{T}}}$. Over the whole of the cruise section, the A_{T} was higher than the C_{T}, with an $A_{\text{T}}/C_{\text{T}}$ ratio ranging from 1.16 to 1.02. Ratios close to 1 and lower pH values correspond to minimum absolute values for the different buffer factors. These were observed in the 1000–1500 m range north of the SAF, and approaching the 250 to 400 m range south of the PF. These minimum values were found in the layer where the AAIW and UCDW were located. They clearly indicate that these water masses are particularly sensitive to increases in $[CO_2]$, and small increases of C_{T} will strongly decrease the pH and the carbonate saturation states.

Mixing processes in the Southern Ocean bring up relatively low $A_{\text{T}}/C_{\text{T}}$ waters that mix with waters where biological production is not able to use up the macronutrients of these HNLC waters and to draw down the inorganic carbon. This results in low $A_{\text{T}}/C_{\text{T}}$ ratios. The pH and saturation states are also highly sensitive to changes in C_{T} and A_{T} in these waters, with values at the end of the austral summer of $\beta_{\text{H}} = 0.36$ mmol kg^{-1} and $\omega_{C_{\text{T}}} = 0.12$ mmol kg^{-1} in surface waters. These are minimum values for both parameters in the ocean, and the chemistry of these surface waters becomes much more sensitive to local variations in both C_{T} and A_{T}.
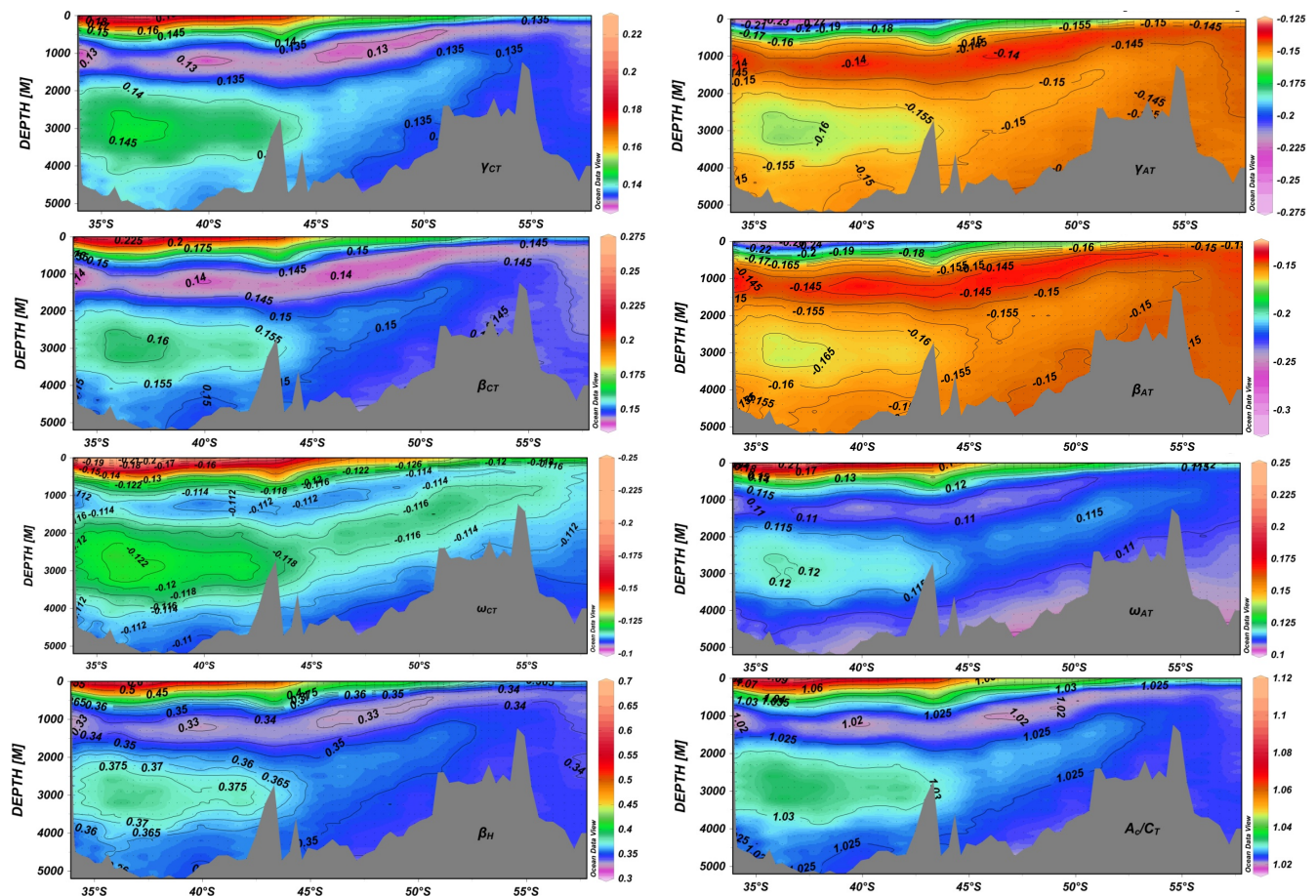
Fig. 5. The vertical distribution of fractional changes in $[CO_2]$ (γ_i), $[H^+]$ (β_i) and Ω (ω_i) (mmol kg^{-1}) over the changes in C_T and A_T and acid-base buffer capacity, β_H, (mmol kg^{-1}) for the whole of the BONUS GoodHope section, together with the ratio of carbonate alkalinity to inorganic carbon A_c/C_T.

Hauck et al. (2010) for the Southern Atlantic Sector and from 56.5° S to 60° S determined an increase in the anthropogenic surface carbon for the period from 1992 to 2008 of between 5.1 and 7.1 µmol kg^{-1} per decade, and lower south of 60° S. Levine et al. (2008) showed, for this same sector, increases of 10–12 µmol kg^{-1} per decade north of 55° S that also decreased to 5–6 µmol kg^{-1} per decade further south. In the Pacific Ocean and along 150° W, Sabine et al. (2008) also found changes in the 10–14 µmol kg^{-1} per decade through to 57° S decreasing to 5–10 µmol kg^{-1} per decade south of 57° S. South of 55° S and at least until 57.5° S, the southernmost place sampled in this work, assuming an increase in C_T due to the uptake of carbon of 10 µmol kg^{-1} ($\Delta A_T = 0$) would increase $[CO_2]$ by 7.1 %, and $[H^+]$ by 6.4 % (a pH decrease of 0.027 units) while the saturation would decrease by 8.1 %. Ω_{cal} would decrease from an actual surface value of 2.35 ± 0.06 to 2.16 ± 0.07 while Ω_{ara} would change from 1.47 ± 0.04 to 1.35 ± 0.05. Assuming an increase in C_T of 5 µmol kg^{-1} per decade as indicated for places further south than 55° S, the pH would decrease by 0.014 units while the

saturation would decrease to 1.41 ± 0.05. Hauck et al. (2010) determined a pH decrease in the first 200 m of 0.016–0.019 per decade for the period from 1992 to 2008 that would account for an increase per decade of C_T by 6–7 µmol kg^{-1}. These calculations clearly indicate that the chemistry of the surface water at high Southern Ocean latitudes will become highly sensitive to variations in C_T (and in A_T if a decrease in calcification takes place) due to increasing CO_2 in the face of future climate change. Assuming the different rates of C_T change as mentioned above, an increase of 10 µmol kg^{-1} per decade will produce aragonite under-saturated surface waters at 55° S in the next 40 yr (by the year 2048). South of 55° S, a lower C_T change between 6 and 7 µmol kg^{-1} increase per decade will produce under-saturation in aragonite by the year 2073 and 2063, respectively. These estimations are in the range of the model predictions (Orr et al., 2005; McNeil and Matear, 2008). A weakening of the CO_2 sink of the Southern Ocean as currently discussed in the literature could not be confirmed by Hauck et al. (2010) and this range of years as determined from our cruise should be updated as more

cruises are produced in the Southern ocean. These same surface waters will be transported equatorwards and subducted into the thermocline near the SAF, forming the highly sensitive AAIW. Furthermore, the results presented in this research provide a basis for comparing the buffering capacity of this region of the Southern Ocean with previous and future cruises and with other oceans.

5 Conclusions

The distribution of carbonate system variables was measured in the Atlantic sector of the Southern Ocean during February and March, 2008. The different frontal systems present in the Southern Ocean have been characterised by considering surface pH variability. The frontal zones were defined by sharp changes in temperature and salinity, high Chl-a accompanied by high pH_{Tis} and minima of $f CO_2$. These characteristics are the result of relatively recent biological activity favoured by upwelling in the presence of cyclonic eddies detached from the Agulhas retroflection region. In other areas, the pH and $f CO_2$ were controlled mainly by hydrographical processes. Over the whole of the section, the pH_{Tis} and $f CO_2$ could be divided in two separate regimes. North of the Subantarctic Front, the SAF, a mean pH_{Tis} value of 8.102 ± 0.014 with $f CO_2$ of $335 \pm 5 \, \mu$atm was observed while to the south the pH_{Tis} was 8.069 ± 0.008 and the $f CO_2$ increased to $365 \pm 10 \, \mu$atm.

The carbonate properties were presented as a function of the different water masses found in the region. In the subtropical zone, the distribution of all the properties was governed by deep anticyclonic and cyclonic features generated by the Agulhas Current System. At the SAF, subduction of the South Atlantic variety of Antarctic Intermediate Water, the AAIW, was identified by the northward deepening of carbonate variables and elevated CFC concentrations. In the Cape Basin area, the Atlantic variety met the Indian AAIW injected with the Agulhas Rings, becoming saltier and warmer but also with a higher content of inorganic carbon than that found at $45°$ S. At greater depths, two North Atlantic Deep Water branches were defined. The first one corresponds to the eastern NADW pathway, with low CFC-12 concentration ($<0.02 \, \mathrm{pmol \, kg^{-1}}$). The second one, encompassing the Antarctic Polar Zone, is associated with the NADW injected in the Antarctic Circumpolar Current in the south-western Argentine Basin with CFC-12 concentrations in the range of 0.08 to 0.1 $\mathrm{pmol \, kg^{-1}}$.

The Antarctic Bottom Water was distinguished by slightly higher CFC-12 concentrations and lower pH_T values, becoming older and more diluted as it spreads northwards to $36°$ S. We could differentiate the two varieties of circumpolar deep water. The Upper waters, the UCDW, composed of low $pH_{T,25}$; and the Lower Circumpolar water, characterised by high salinity and $pH_{T,25}$. Both are characterised by maxima in C_T, attributed to the influence of old waters from the Indian and Pacific Oceans.

The Southern Ocean is known to be very sensitive to changes in carbonate chemistry. Seven buffer indices that relate changes in C_T and A_T to changes in [CO_2], [H^+] and calcium carbonate saturation states showed low values, i.e., low buffering capacity and highly sensitive waters with future increases of CO_2. The lowest values were observed in the 1000–1500 m range north of the SAF, and the 250 to 400 m range south of the Polar Front. These depth ranges correspond to the water layer where the AAIW and UCDW are located, both of which together with the whole section are particularly sensitive to increases in atmospheric CO_2. Strong decreases in pH and in the calcium carbonate saturation states were observed at the present rate of change in the oceanic carbon dioxide scenario for the Southern Ocean surface seawater. We predicted that under present per decade CO_2 increases, the surface water from the year 2048 (at around $55°$ S) to 2073 (further south than $55°$ S) will be undersaturated in aragonite.

References

Arhan, M., Mercier, H., and Park, Y.-H.: On the Deep Water circulation of the eastern South Atlantic Ocean, Deep-Sea Res. Pt. I, 50, 889–916, 2003.

Arhan, M., Speich, S., Dencausse, G., Messager, C., Fine, R., and Boye, M.: Anticyclonic and cyclonic eddies of subtropical origin in the subantarctic zone south of Africa, J. Geophys. Res. Oceans, submitted, 2011.

Bakker, D. C. E., de Baar, H. J. W., and Bathmann, U. V.: Changes of carbon dioxide in surface-waters during spring in the Southern Ocean, Deep-Sea Res. Pt. II, 44, 91–128, 1997.

Bakker, D. C. E., Hoppema, M., Schröder, M., Geibert, W., and de Baar, H. J. W.: A rapid transition from ice covered CO_2 rich waters to a biologically mediated CO_2 sink in the eastern Weddell Gyre, Biogeosciences, 5, 1373–1386, doi:10.5194/bg-5-1373-2008, 2008.

Belkin, I. M. and Gordon, A. L.: Southern Ocean fronts from the Greenwich meridian to Tasmania, J. Geophys. Res., 101, 3675–3696, 1996.

Boebel, O., Rossby, T., Lutjeharms, J., Zenk, W., and Barron, C.: Path and variability of the Agulhas Return Current, Deep-Sea Res. II, 50, 35–56, 2003.

Borges, A. V., Tilbrook, B., Metzl, N., Lenton, A., and Delille, B.: Inter-annual variability of the carbon dioxide oceanic sink south of Tasmania, Biogeosciences, 5, 141–155, doi:10.5194/bg-5-141-2008, 2008.

Branellec P., Arhan, M., and Speich, S.: Projet GoodHope, Campagne BONUS/GOODHOPE, Rapport de données CTD-O2, IFREMER Report OPS/LPO/10-02, 282 pp., 2010.

Brévière, E., Metzl, N., Poisson, A., and Tilbrook, B.: Changes of the oceanic CO_2 sink in the Eastern Indian sector of the Southern Ocean, Tellus, 58B, 438–446, 2006.

Bullister J. L. and Weiss, R. F.: Determination of CCl_3F and CCl_2F_2 in seawater and air, Deep-Sea Res. 35, 839–853, 1988.

Caldeira K., and Wickett M. E.: Anthropogenic carbon and ocean pH, Nature, 425, 365–365, 2003.

Chever, F., Bucciarelli, E., Sarthou, G., Speich, S., Arhan, M., Penven, P., and Tagliabue, A.: Physical speciation of iron in the Atlantic sector of the Southern Ocean, along a transect from the subtropical domain to the Weddell Sea Gyre, J. Geophys. Res. Ocean, 115(10), C10059, doi:10.1029/2009JC005880, 2010.

Chierici, M., Fransson, A., Turner, D. R., Pakhomov, E. A., and Froneman, P. W.: Variability in pH, $f CO_2$, oxygen and flux of CO_2 in the surface water along a transect in the Atlantic sector of the Southern Ocean, Deep-Sea Res. Pt. II, 51, 2773–2787, 2004.

Clayton, T. D. and Byrne, R. H.: Spectrophotometric seawater pH measurements: total hydrogen ion concentration scale calibration of m-cresol purple and at-sea results, Deep Sea Res. Pt. I, 40, 2115–2129, 1993.

Crawford, W. R., Brickley, P. J., Petersonc, T. D., and Thomas, A. C.: Impact of Haida Eddies on chlorophyll distribution in the Eastern Gulf of Alaska, Deep-Sea Res. II, 52, 975–989, 2005.

Dencausse, G., Arhan, M., and Speich, S.: Spatio-temporal characteristics of the Agulhas Current retroflection, Deep Sea Res. Pt. 1, 57, 1392–1405, 2010.

Dickson, A. G.: Standard potential of the reaction: AgCl(s) + 1/2 H2(g) = Ag(s) + HCl(aq), and the standard acidity constant of the ion HSO_4^- in synthetic seawater from 273.15 to 318.15 K, J. Chem. Thermodyn., 22, 113–127, 1990a.

Dickson, A. G.: Thermodynamics of the dissociation of boric acid in synthetic seawater from 273.15 to 318.15 K, Deep-Sea Res., 37, 755–766, 1990b.

Dickson, A. G. and Millero, F. J.: A comparison of the equilibrium constants for the dissociation of carbonic acid in seawater media, Deep-Sea Res., 34, 1733–1743, 1987.

Egleston, E. S., Sabine, C. L., and Morel, F. M. M.: Revelle revisited: Buffer factors that quantify the response of ocean chemistry to changes in DIC and alkalinity, Global Biogeochem. Cy., 24, GB1002, doi:10.1029/2008GB003407, 2010.

Fine, R. A., Warner, M. J., and Weiss, R. F.: Water mass modification at the Agulhas Retroflection: Chlorofluoromethane Studies, Deep-Sea Res., 35, 311–332, 1988.

Frankignoulle, M.: A complete set of buffer factors for acid/base CO_2 system in seawater, J. Mar. Sys., 5, 111–118, 1994.

Friis, K., Körtzinger, A., and Wallace, D. W. R.: The salinity normalization of marine inorganic carbon chemistry data, Geophys. Res. Lett., 33(2), 1085, doi:10.1029/2002GL015898, 2003.

Gladyshev, S., Arhan, M., Sokov, A., and Speich, S.: A hydrographic section from South Africa to the southern limit of the Antarctic Circumpolar Current at the Greenwich meridian, Deep-Sea Res. Pt. I, 55, 1284–1303, 2008.

Gonzalez-Dávila, M., Santana-Casiano, J. M., Rueda, M. J., Llinás, O., and Gonzalez-Dávila, E. F.: Seasonal and interannual variability of seasurface carbon dioxide species at the European Station for Time Series in the Ocean at the Canary Islands (ESTOC) between 1996 and 2000, Global Biogeochem. Cy., 17(3), 1076, doi:10.1029/2002GB001993, 2003.

González-Dávila, M., Santana-Casiano, J. M., de Armas, D., Escánez, J., and Suarez-Tangil, M.: The influence of island generated eddies on the carbon dioxide system south of the Canary Islands, Mar. Chem., 99, 177–190, 2006.

Hauck, J., Hoppema, M., Bellerby, R. G. J., Völker, C., and Wolf-Gladrow, D.: Data-based estimation of anthropogenic carbon and acidification in the Weddell Sea on a decadal timescale, J. Geophys. Res., 115, C03004, doi:10.1029/2009JC005479, 2010.

Hoppema, M., Fahrbach, E., Schröder, M., Wisotzki, A., and de Baar, H. J. W.: Winter-summer differences of carbon dioxide and oxygen in the Weddell Sea surface layer, Mar. Chem., 51, 177–192, 1995.

Hoppema, M., Stoll, M. H. C., and de Baar, H. J. W.: CO_2 in the Weddell Gyre and Antarctic Circumpolar Current: Austral autumn and early winter, Mar. Chem., 72, 203–220, 2000.

Key, R. M., Kozyr, A., Sabine, C. L., Lee, K., Wanninkhof, R., Bullister, J. L., Feely, R.A., Millero, F.J., Mordy, C., and Peng, T.-H.: A global ocean carbon climatology: Results from Global Data Analysis Project (GLODAP), Global Biogeochem. Cy., 18, GB4031, doi:10.1029/2004GB002247, 2004.

Laika, H. E., Goyet, C., Vouve, F., Poisson, A., and Touratier, F.: Interannual properties of the CO_2 system in the southern ocean south of Australia, Antarctic Sci., 21(6), 663–680, 2009.

Lee, K., Tong, L. T., Millero, F. J., Sabine, C. L., Dickson, A. G., Goyet, C., Park, G.-H., Wanninkhof, R., Feely, R. A., and Key, R. M.: Global relationships of total alkalinity with salinity and temperature in surface waters of the world's oceans, Geophys. Res. Lett., 33, L19605, doi:10.1029/2006GL027207, 2006.

Levine, N. M., Doney, S. C., Wanninkhof, R., Lindsay, K., and Fung, I. Y.: Impact of ocean carbon system variability on the detection of temporal increases in anthropogenic CO_2, J. Geophys. Res., 113, C03019, doi:10.1029/2007JC004153, 2008.

Lewis, E. and D. W. R. Wallace.: Program Developed for CO2 System Calculations. ORNL/CDIAC-105. Carbon Dioxide Information Analysis Center, Oak Ridge National Laboratory, U.S. Department of Energy, Oak Ridge, Tennessee, 1998.

Lo Monaco C., Metzl, N., Poisson, A., Brunet, C., and Schauer B.: Anthropogenic CO_2 in the Southern Ocean: Distribution and inventory at the Indian-Atlantic boundary (World Ocean Circulation Experiment line I6), J. Geophys. Res., 110, C06010, doi:10.1029/2004JC002643, 2005.

Lutjeharms, J. R. E. and Valentine, H. R.: Southern Ocean thermal fronts south of Africa, Deep-Sea Res. Pt. I, 31, 1461–1475, 1984.

Lovenduski, N. S. and Gruber, N.: The impact of the Southern Annular Mode on Southern Ocean circulation and biology, Geophys. Res. Lett., 32, L11603, doi:10.1029/2005GL022727, 2005.

Mantisi, F., Beauverger, C., Poisson, A., and Metzl, N.: Chlorofluoromethanes in the western Indian sector of the Southern Ocean and their relations with geochemical tracers, Mar. Chem., 35, 151–167, 1991.

Mehrbach, C., Culberson, C. H., Hawlay, J. E., and Pytkowicz, R. M.: Measurement of the apparent dissociation constants of carbonic acid in seawater at atmospheric pressure, Limnol.

Oceanogr., 18, 897–907, 1973.

McGillicuddy Jr., D. J., Anderson, L. A., Doney, S. C., and Maltrud, M. E.: Eddy-driven sources and sinks of nutrients in the upper ocean: results from a 0.18 resolution model of the North Atlantic, Global Biogeochem. Cy., 17(2), 1035, doi:10.1029/2002GB001987, 2003.

McNeil, B. I. and Matear, R. J.: Climate change feedbacks on future oceanic acidification, Tellus B, 59, 191–198, 2007.

McNeil, B. I. and Matear, R. J.: Southern Ocean acidification: A tipping point at 450-ppm atmospheric CO_2, P. Natl. Acad. Sci. USA, vol. 105(48), 18860–18864, 2008.

McNeil, B. I., Metzl, N., Key, R. M., Matear, R. J., and Corbiere, A.: An empirical estimate of the Southern Ocean air-sea CO_2 flux, Global Biogeochem. Cy., 21, GB3011, doi:10:1029/2007GB002991, 2007.

Metzl, N., Poisson, A., Louanchi, F., Brunet, C., Shauer, B., and Brès, B.: Spatio-temporal distribution of air-sea fluxes of CO_2 in the Indian and Antarctic oceans, Tellus, 47B, 56–69, 1995.

Mintrop, L., Pérez, F. F., González Dávila, M., Körtzinger, A., and Santana-Casiano, J. M.: Alkalinity determination by potentiometry: intercalibration using three different methods, Cien. Mar., 26, 23–37, 2000.

Mucci, A.: The solubility of calcite and aragonite in seawater at various salinities, temperatures, and one atmosphere total pressure, Am. J. Sci., 283, 781–799, 1983.

Orr, J. C, Fabry, V. J., Aumont, O., Bopp, L., Doney, S. C., Feely, R. A., Gnanadesikan, A., Gruber, N., Ishida, A., Joos, F., Key, R. M., Lindsay, K., Maier-Reimer, E., Matear, R., Monfray, P., Mouchet, A., Raymond, G., Najjar, R. G, Plattner, G.-K., Rodgers, K. B., Sabine, C. L., Sarmiento, J. L., Schlitzer, R., Slater, R. D., Totterdell, I. J., Weirig, M.-F., Yamanaka, Y., and Yool, A.: Anthropogenic ocean acidification over the twenty-first century and its impact on calcifying organisms, Nature, 437, doi:10.1038/nature04095, 681–686, 2005.

Orsi, A. H. and Whitworth III, T.: Hydrographic atlas of the world ocean circulation experiment (WOCE), in: Southern Ocean, vol. 1, International WOCE project Office, edited by: Sparrow, M., Chapman, P., and Gould, J., International WOCE Project Office Southampton, UK, ISBN 0-904175-49-9, 2005.

Orsi, A. H., Smethie Jr., W. M., and Bullister, J. L.: On the total input of Antarctic waters to the deep ocean: A preliminary estimate from chlorofluorocarbon measurements, J. Geophys. Res., 107(C8), 3122, doi:10.1029/2001JC000976, 2002.

Park, Y.-H., Charriaud, E., and Craneguy, P.: Fronts, transport, and Weddell Gyre at 30°E between Africa and Antarctica, J. Geophys. Res., 106, 2857–2879, 2001.

Pelegri, J. L., Aristegui, J., Cana, L., Gonzalez-Davila, M., Hernandez-Guerra, A., Hernandez-Leon, S., Marrero-Diaz, A., Montero, M. F., Sangra, P., and Santana-Casiano, J. M.: Coupling between the open ocean and the coastal upwelling region off northwest Africa: water recirculation and offshore pumping of organic matter, J. Mar. Syst., 54, 3–37, 2005.

Richardson, P. L.: Agulhas leakage into the Atlantic estimated with subsurface floats and surface drifters, Deep-Sea Res. I, 54, 1361–1389, 2007.

Richardson, P. L., Lutjeharms, J. R. E., and Boebel, O.: Introduction to the "inter-ocean exchange around southern Africa", Deep-Sea Res. Pt. II, 50, 1–12, 2003.

Sabine, C. L., Feely, R. A., Millero, F. J., Dickson, A. G., Langdon, C., Mecking, S., and Greeley, D.: Decadal changes in Pacific carbon, J. Geophys. Ress, 113, C07021, doi:10.1029/2007JC004577, 2008.

Santana-Casiano, J. M. and González-Dávila, M.: pH decrease and effects on the chemistry of seawater, in: Oceans and the Atmospheric Carbon Content, edited by: Duarte P. and Santana-Casiano, J. M., Spinger, Dordrecht, 95–114, 2011.

Sarmiento, J. L., Hughes, T. M. C., Stouffer, R. J., and Manabe, S.: Simulated response of the ocean carbon cycle to anthropogenic climate warming, Nature, 393, 245–249, 1998.

Siegenthaler, U. and Sarmiento, J. L.: Atmospheric carbon dioxide and the ocean, Nature, 365, 119–125, 1993.

Smith, W. O. and Nelson, D. M.: Importance of ice edge phytoplankton production in the Southern Ocean, Bioscience, 36, 251–257, 1986.

Smith, W. O. and Nelson, D. M.: Phytoplankton growth and new production in the Weddell Sea marginal ice zone during austral spring and autumn, Limnol. Oceanogr., 35, 809–821, 1990.

Speich, S. and Dehairs, G.: Cruise Report, MD 66 BONUS-GOODHOPE, Internal Report, 246 pp., 2008.

Speich, S., Arhan, M., Gladyshev, S., Rupolo, V., and Perrot, X.: Upper layer structure and dynamics along BGH, Ocean Sci., submitted, 2011.

Toggweiler, J. R., Russell, J. L., and Carson, S. R.: Mid-latitude westerlies, atmospheric CO_2 and climate change during the ice ages, Paleoceanography, 21, PA2005, doi:10.1029/2005PA001154, 2006.

Van Aken, H. M., van Veldhoven, A. K., Veth, C., de Ruijter, W. P. M., van Leeuwen, P. J., Drijfhout, S. S., Whittle, C. P., and Rouault, M.: Observation of a young Agulhas ring, Astrid, during MARE in March 2000, Deep-Sea Res. Pt. II, 50, 167–195, 2003.

Venables, H. and Moore, M.: Phytoplankton and light limitation in the southern ocean: learning from high-nutrient, high-chlorphyll areas, J. Geophys. Res., 115, C02015, doi:10.1029/2009JC005361, 2010.

Whitworth, T. and Nowlin, W. D.: Water masses and currents of the Southern Ocean at the Greenwich Meridian, J. Geophys. Res., 92, 6462–6476, 1987.

Wong, A. P. S., Bindoff, N. L., and Forbes, A.: Ocean-ice shelf interaction and possible bottom water formation in Prydz Bay, Antarctica, Antarct. Res. Ser., 75, 173–187, 1998.